Micromechanical properties of hydrogels measured with MEMS resonant sensors

Elise A. Corbin, Larry J. Millet, James H. Pikul, Curtis L. Johnson, John G. Georgiadis, William P. King & Rashid Bashir

Biomedical Microdevices
BioMEMS and Biomedical Nanotechnology

ISSN 1387-2176

Biomed Microdevices
DOI 10.1007/s10544-012-9730-z

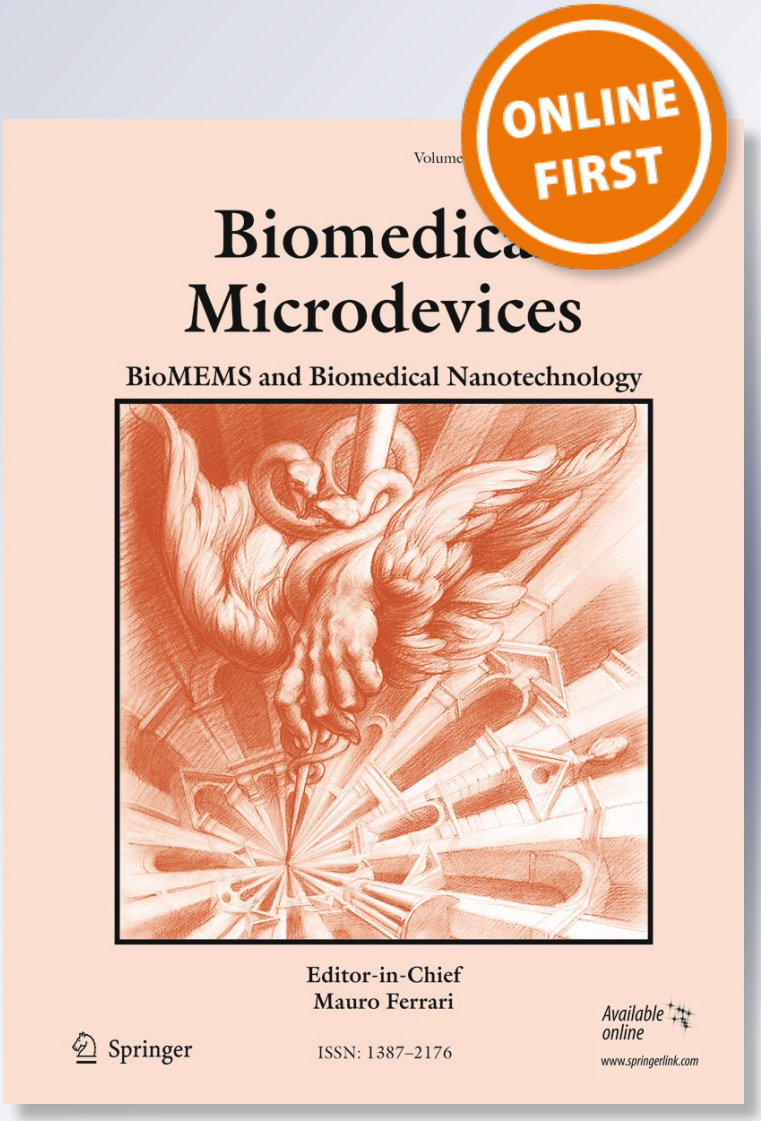

Springer

Biomed Microdevices
DOI 10.1007/s10544-012-9730-z

Micromechanical properties of hydrogels measured with MEMS resonant sensors

Elise A. Corbin · Larry J. Millet · James H. Pikul · Curtis L. Johnson · John G. Georgiadis · William P. King · Rashid Bashir

Abstract Hydrogels have gained wide usage in a range of biomedical applications because of their biocompatibility and the ability to finely tune their properties, including viscoelasticity. The use of hydrogels on the microscale is increasingly important for the development of drug delivery techniques and cellular microenvironments, though the ability to accurately characterize their micromechanical properties is limited. Here we demonstrate the use of microelectromechanical systems (MEMS) resonant sensors to estimate the properties of poly(ethylene glycol) diacrylate (PEGDA) microstructures over a range of concentrations. These microstructures are integrated on the sensors by deposition using electrohydrodynamic jet printing. Estimated properties agree well with independent measurements made using indentation with atomic force microscopy.

Keywords MEMS mass sensor · Electrohydrodynamic jet printing · Polyethylene glycol · Mass-spring-damper system · Hydrogel micromechanics

E. A. Corbin · J. H. Pikul · C. L. Johnson · J. G. Georgiadis · W. P. King
Department of Mechanical Science and Engineering,
University of Illinois Urbana-Champaign,
Urbana, IL 61801, USA

E. A. Corbin · L. J. Millet · W. P. King · R. Bashir
Micro and Nanotechnology Laboratory,
University of Illinois Urbana-Champaign,
Urbana, IL 61801, USA

R. Bashir (✉)
Department of Electrical and Computer Engineering,
University of Illinois Urbana-Champaign,
Urbana, IL 61801, USA
e-mail: rbashir@illinois.edu

1 Introduction

Hydrogels are critically important to many biomedical applications (Liang et al. 2011) including drug delivery (Kolambkar et al. 2011) and tissue engineering (Nicodemus and Bryant 2008) due to their biocompatibility and mechanical properties. Hydrogel stiffness can be controlled to mimic a desired tissue microenvironment, enabling hydrogel tissue scaffolds that have mechanical behavior similar to that of extracellular matrix. (Drury and Mooney 2003) There is, however, a lack of understanding of the micromechanical behavior of hydrogels and a need for suitable methods to probe this behavior. (Anseth et al. 1996; Peppas et al. 2006) In particular, it is difficult to make quantitative *in situ* mechanical property measurements because the elastic and viscous properties of hydrogels can vary over several orders of magnitude depending on composition, concentration, and swelling. (Kim et al. 2009; Yoon et al. 2010) A deeper understanding of how to control and measure hydrogel mechanical properties is required in order to engineer cellular microenvironments.

Hydrogels are used for both macroscopic (Jeong et al. 2012) and microscopic cellular environments. (Chan et al. 2010) Therapeutic vascularization techniques for regenerative medicine rely on macroscopic templates of hydrogels with micro-patterns and embedded angiogenic factors. (Phelps et al. 2010; Jeong et al. 2012) 3D cell encapsulation with hydrogels can guide cellular processes such as differentiation. (Chan et al. 2010) Hydrogels have also been developed for layering on the inner surface of blood vessels to control timed drug release for intravascular localized drug delivery. (Slaughter et al. 2009) At the macroscale, the mechanical properties

Published online: 18 December 2012

of hydrogels can be measured using dynamic mechanical analysis, (Anseth et al. 1996) oscillatory shear rheometry, (Ulrich et al. 2009) and elastography. (Sack et al. 2001) Much less work has been published on the mechanical properties of hydrogels at the micrometer scale. Atomic force microscopy (AFM) measurements can obtain the hardness of soft biological materials, but data interpretation is difficult due to the complex geometry of the AFM tip. (Kurland et al. 2012) A quartz crystal microbalance (QCM) can estimate the viscoelasticity of materials in an aqueous environment, but samples are limited to uniform thin films with macroscopic diameters that depend on QCM electrode size. Ideally, micrometer scale hydrogel mechanical property measurements would include: measurements on microscopic amounts of hydrogel; the measurement of both elastic and viscous properties, both of which can vary significantly with hydrogel composition; hydrogel characterization in a liquid environment; and hydrogels that have been integrated on a microscopic lab-on-chip platform.

We propose to measure the viscoelastic properties of hydrogels using microelectromechanical system (MEMS) resonant sensors. These sensors have traditionally enabled mass measurement of a range of biomaterials, such as viruses, (Lee et al. 2008) bacteria, (Gupta et al. 2004) cells, (Burg et al. 2007; Park et al. 2008, 2010) biochemicals, (Burg et al. 2007) and polymers. (Millet et al. 2012) Resonant sensors rely on the technique of measuring frequency shift, where the difference in resonant frequency between an unloaded sensor and a sensor loaded with a sample reflects the adhered mass. However, if the material is soft, such as with hydrogels, it introduces a complicated coupled-oscillator effect where the material will oscillate relative to the sensor, and the measured resonant frequency depends on the viscoelasticity of the material in addition to its mass. The coupled-oscillator effect can be described by a two degree-of-freedom (2DOF) dynamic system, which is used to estimate the viscoelasticity of soft materials through apparent mass measurements with the MEMS resonant sensor.

This paper describes the measurement of the elastic and viscous properties of nanogram-scale samples of poly(ethylene glycol) diacrylate (PEGDA) hydrogel samples (MW 575 g mol^{-1}) that have been integrated onto a MEMS resonant sensor. Because it is difficult to attach prefabricated hydrogels individually to the surface of each suspended sensor the gels must be fabricated directly onto the devices. Here we use electrohydrodynamic jet (e-jet) printing, (Park et al. 2007) which uses high electric fields to pattern liquids onto grounded substrates, for integrating hydrogels onto our fully suspended MEMS resonant sensor. The mechanical properties of cross-linked PEGDA hydrogel structures are tunable by varying the polymer concentration, (Nemir et al. 2010) and the properties of samples prepared with 5–20% hydrogel concentration are investigated in this paper.

2 Results and discussion

The MEMS resonant sensor used in this study consists of a 60x60 μm^2 platform suspended by four micro beam-springs to provide uniform mass sensitivity across the sensor (Park et al. 2010, 2012). Figure 1 shows an overview of the typical mass measurement with the sensor. Our measurement uses electromagnetic actuation and a laser Doppler vibrometer (LDV) system to measure the velocity of the vibrating platform in conjunction with a feedback loop and a lock-in amplifier to iteratively determine the resonant frequency (Fig. 1a). Measurement of the resonant frequency of the sensor with an adhered material, and comparison with that of an empty sensor, allows for the mass of the material to be calculated. The resonance condition is also dependent on the viscoelastic properties of the adhered material, which becomes significant with soft materials and skews the apparent measured mass. By treating the model as a Kelvin-Voigt viscoelastic solid, (Fung 1981) the sensor with adhered solid was modeled as the 2DOF spring-mass-damper dynamic system shown in Fig. 1b (Park et al. 2010). Figure 1c shows predictions using the model of how the ratio of apparent mass to actual mass changes over a range of mechanical properties.

To establish a baseline for the hydrogel properties, we used AFM to measure the elastic and viscous properties of hydrogel samples while submerged in DI water. AFM analysis utilized thin film hydrogel samples with thickness of approximately 70 μm created by cross-linking pre-polymer with a 365 nm UV light source. We used a silicon nitride cantilever with a spring constant of 0.06 N m^{-1} and a 2.5 μm silica spherical-tip. Force-indentation curves coupled with the Hertz contact mechanics model determined the elastic moduli of hydrogels at each PEGDA concentration (Fig. 2a). Fitting used the linear elastic deformation region of the curve, and a low loading rate was selected to minimize viscous effects in this region. (A-Hassan et al. 1998; Engler et al. 2007; Li et al. 2008; Nawaz et al. 2012) For each sample, we measured approximately ten locations across the surface and averaged, with the resulting elastic modulus ranging from 2.84 to 228.94 kPa, for 5% to 20% concentration (Table 1).

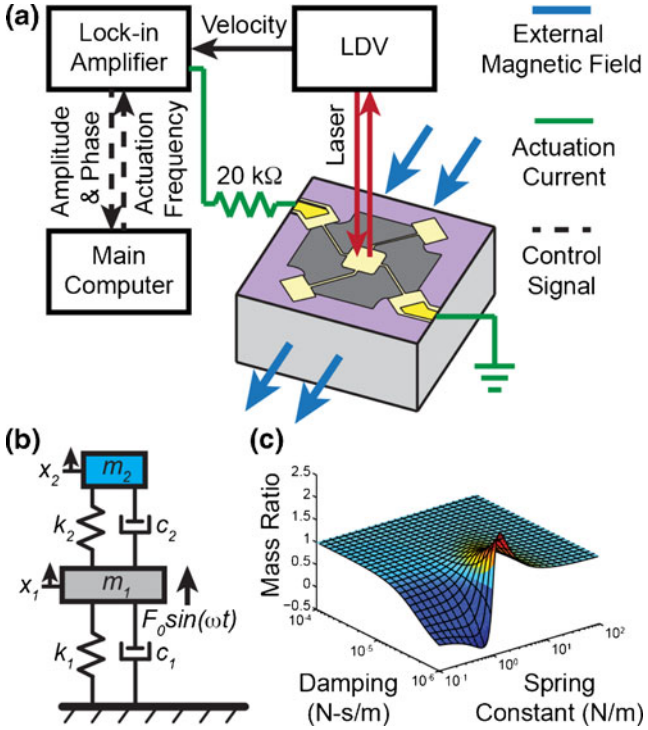

Fig. 1 Overview of the measurement approach. **a** Schematic summarizing the frequency measurement setup. **b** Schematic of the free body diagram of 2-degree-of-freedom (2DOF) dynamic model, where m_1, k_1, c_1, and x_1 are the mass, spring constant, damping, and displacement of the sensor, and m_2, k_2, c_2, and x_2 are the mass, spring constant, damping, and displacement of the adhered object. **c** Three-dimensional model plot summarizing how the spring constant and damping of the object influence mass measurement (mass ratio is apparent mass divided by actual mass)

We also used AFM to determine the viscosity of the hydrogel structures through creep experiments, where we applied an instantaneous load and then held for 10 s, while monitoring the deformation (Fig. 2b). Utilizing a Kelvin-Voigt viscoelastic model we can extract the viscosity for each sample, (Vadillo-Rodriguez et al. 2009) again averaged over ten measurements, with the resulting viscosity ranging from 0.2 to 5.1 mPa s (Table 1). The measurement of the viscosity of the 5% hydrogel was problematic due to the challenges of performing AFM creep measurements on low viscosity materials. For analysis and display we assumed a viscosity value of 1.0 mPa-s for the 5% hydrogel corresponding to water at 20 °C. Note that this value does not alter the findings using the resonant sensor as described later.

The measured elastic modulus, E, and viscosity, η, of a hydrogel solid exhibit a power-law dependence on hydrogel concentration. Previous work has indicated that the elasticity of hydrogels is proportional to the square of the concentration, while other studies have shown the power-law exponent to vary depending on the type of hydrogel. (Normand et al. 2000; Kong et al. 2003) To determine the power-law behavior of both E and η for the PEGDA hydrogels, the experimental AFM data was fitted in a least-squares fashion for a range of exponents. Coefficient of determination (R^2) was used to determine goodness of fit, and the exponent with maximum goodness of fit was chosen and the corresponding coefficient was recorded. For E, the values found were:

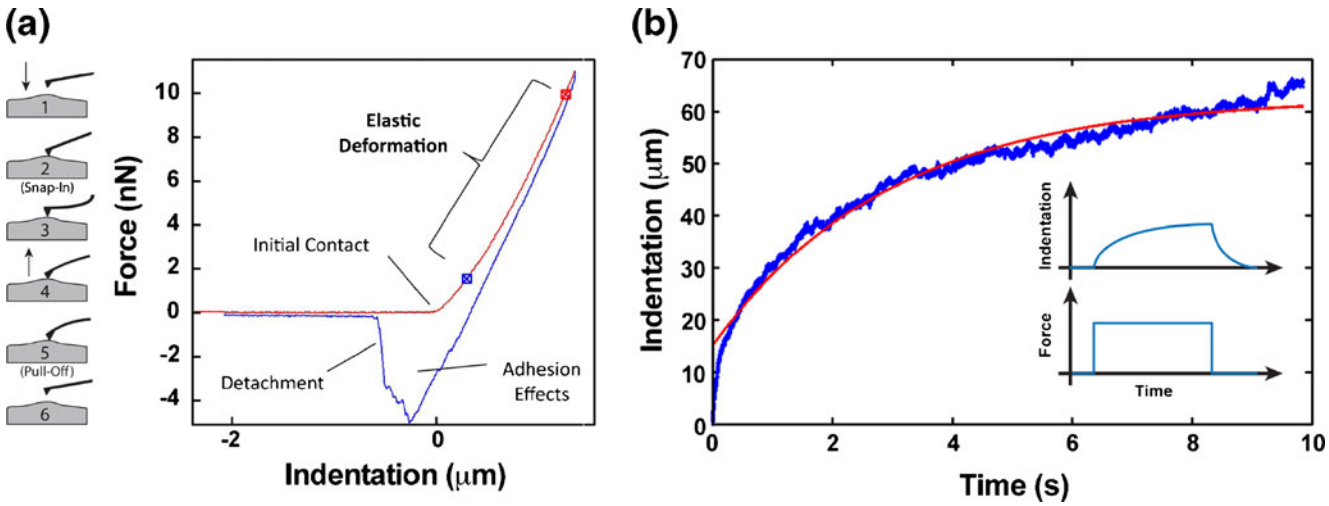

Fig. 2 Overview of the atomic force microscopy mechanical property measurements. **a** Force-indentation measurement cartoon, where the cantilever probe is brought down into contact, and pushed into the surface to a set force and the retracted from the surface until the cantilever is fully detached. Example raw data of the force-indentation curve depicting the elastic deformation region. **b** Creep measurement inset shows the applied load vs. time and the indentation response vs. time. Example raw data of the indentation-time curve depicting the curve fit for the data set

Table 1 AFM data of viscoelastic measurements of all polymer solution concentrations. Note that the measured viscosity of the 5% concentration samples are unreliable due to challenges of performing AFM creep measurements on low viscosity materials

Polymer Solution Concentration (%)	Density (g mL^{-1})	Elastic Modulus (kPa)	Viscosity (mPa-s)
5	1.0062	2.8	NA
10	1.0124	44.6	2.1
15	1.0186	137.0	3.7
20	1.0248	228.9	5.1

a=2.16 and E_0=7.54 MPa (R^2=0.9904). For η, the values found were: b=2.01 and η_0=108.74 mPa·s (R^2=0.9883).

Nanogram-scale hydrogel samples were integrated onto the resonant microsensors using e-jet printing, which is advantageous in its superior resolution to conventional printing techniques (Park et al. 2007; Pikul et al. 2011). Figure 3a shows the e-jet printing procedure, which uses electric fields to print small volumes of liquid onto a substrate with precision placement. The electric field causes charge in the hydrogel solution to accumulate at the liquid surface. The Coulombic repulsion of the surface charge balances with surface tension causing the meniscus at the nozzle end to deform into a conical shape, called a Taylor cone. When the electric field exceeds a critical limit, the stress from the surface charge repulsion at the cone apex exceeds the surface tension and a droplet of fluid is emitted towards the grounded substrate. We deposited the pre-polymer as single droplets, with a predefined diameter and position, and immediately photopolymerized and stored the gels in DI water for equilibration. Figure 3b shows a differential interference contrast microscopy image of a deposited hydrogel structure on a sensor.

In order to determine the volume of the deposited hydrogel samples, we used confocal microscopy to image the fluorescently-coated (fluorescein isothiocyanate-conjugated poly-L-lysine) surface of the gel in water. Figure 3c shows an example of confocal images of the hydrogels, from which we estimated the volume of each structure using Amira 5.4.1 (Visualization Sciences Group; Mérignac, France). Figure 3d shows the gel volume reconstruction, which was performed by manually selecting the dark voxels on each slice and combining all processed slices to render the hydrogel volume. Multiplying the reconstructed volumes with the hydrogel density returned the volumetric mass for each hydrogel sample.

Following the deposition of hydrogels on the sensor platform, we measured the apparent mass of each

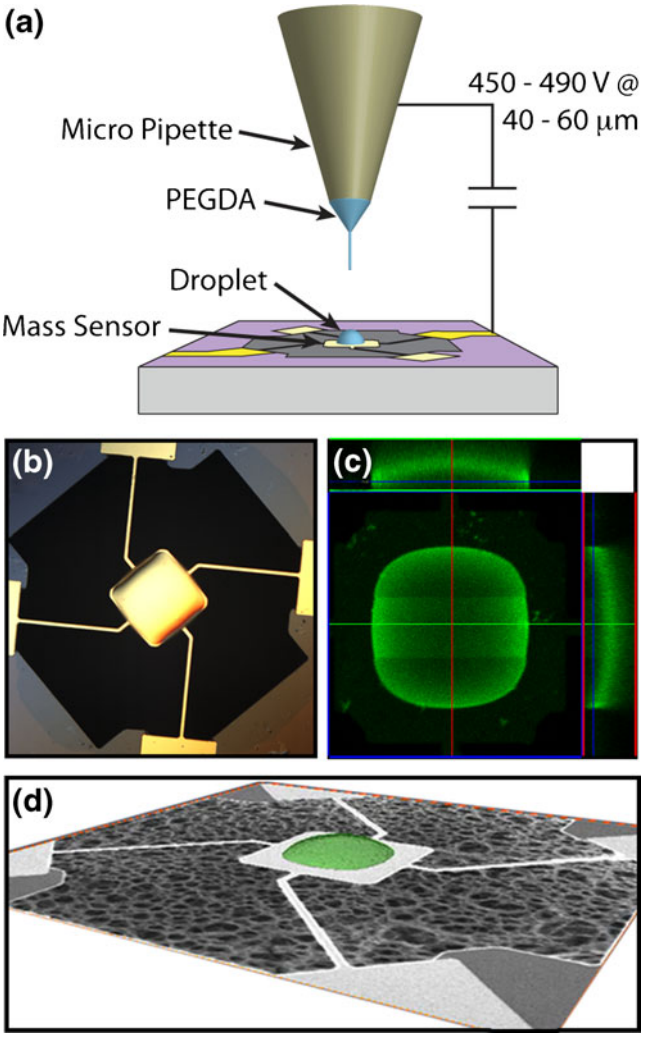

Fig. 3 **a** Schematic of the electrohydrodynamic jet printing setup consisting of a micropipette coated with gold-palladium attached to a syringe with a variable back-pressure input. PEGDA hydrogels were deposited at a separation distance of 40–60 μm with base and peak voltages of 450V and 490V, respectively, and a 0.1% duty cycle. **b** Confocal image of the PEGDA structure on a sensor coated with poly-L-lysine. **c** Differential interference contrast image of PEGDA on a sensor. **d** Hydrogel volume reconstruction using Amira overlaid on SEM image of sensor

structure with the resonant sensors and LDV system. This apparent mass is compared with the volumetric mass calculated using confocal microscopy, which we refer to as "actual" mass. Figure 4a shows the apparent mass and the actual mass for 5% and 10% gels with fitted slope lines, which describes the apparent mass ratio. As expected, the apparent mass is not equal to the actual mass, with the 5% gels appearing less than actual and 10% gels appearing greater than actual. For hydrogels of higher concentration, the mass ratio was close to 1. The apparent mass ratio for each hydrogel concentration was 0.765, 1.112, 0.993, and 1.018 for the 5%, 10%, 15%, and

20% gels, respectively. These ratios highlight the strong dependence of apparent mass as measured by resonant sensors on the mechanical properties of the material, which is especially true for soft materials. As elastic modulus increases, the adhered sample behaves more like a point mass and the coupled oscillator effect is minimized, thus the resonant sensor returns the true mass.

Figure 4b shows a 2D contour view of the mass ratio predicted by the model for a range of elastic moduli and viscosities, with the locations of each gel percentage indicated by a red dot and a line indicating a cut through the measured points. Figure 4c shows the predicted values from the model along this line, as well as the experimental data points, which exhibit strong agreement with the model. These results indicate that the 2DOF model reliably captures the dependence of apparent mass ratio on viscoelastic properties of the material.

The validated model can now be used for the inverse calculation of the hydrogel samples mechanical properties from the apparent mass measured from the sensor. The inverse calculation uses the mass ratio data of the apparent mass read by the sensor and the actual mass on the sensor. The calculation procedure uses the model to formulate an error term for each measured structure as a function of unknown elastic modulus and viscosity. By recognizing that the mechanical properties of hydrogels obey a power-law dependence on concentration, we were able to simultaneously solve for power-law coefficients and exponents for both elastic modulus and viscosity using all samples together. These power-law values extracted from AFM data are the initial guesses for the iterative property estimation procedure.

Figure 5 presents the elastic moduli and viscosities measured with AFM along with the power-law behavior estimated with the resonant sensors this technique. The estimated power-law exponent is 2.07 and power-law coefficient is 8.37 MPa for elastic modulus. The estimated elastic moduli of the hydrogels are somewhat higher than the values measured with AFM, though they still show very good agreement (R^2=0.7783) and are consistent with previous work on PEGDA MW 575 g mol^{-1} hydrogels. (Keim and Gall 2010) For viscosity, the estimated power-law exponent is 1.90 and power-law coefficient is 88.83 mPa-s, and this behavior exhibited excellent agreement with AFM data (R^2=0.9867).

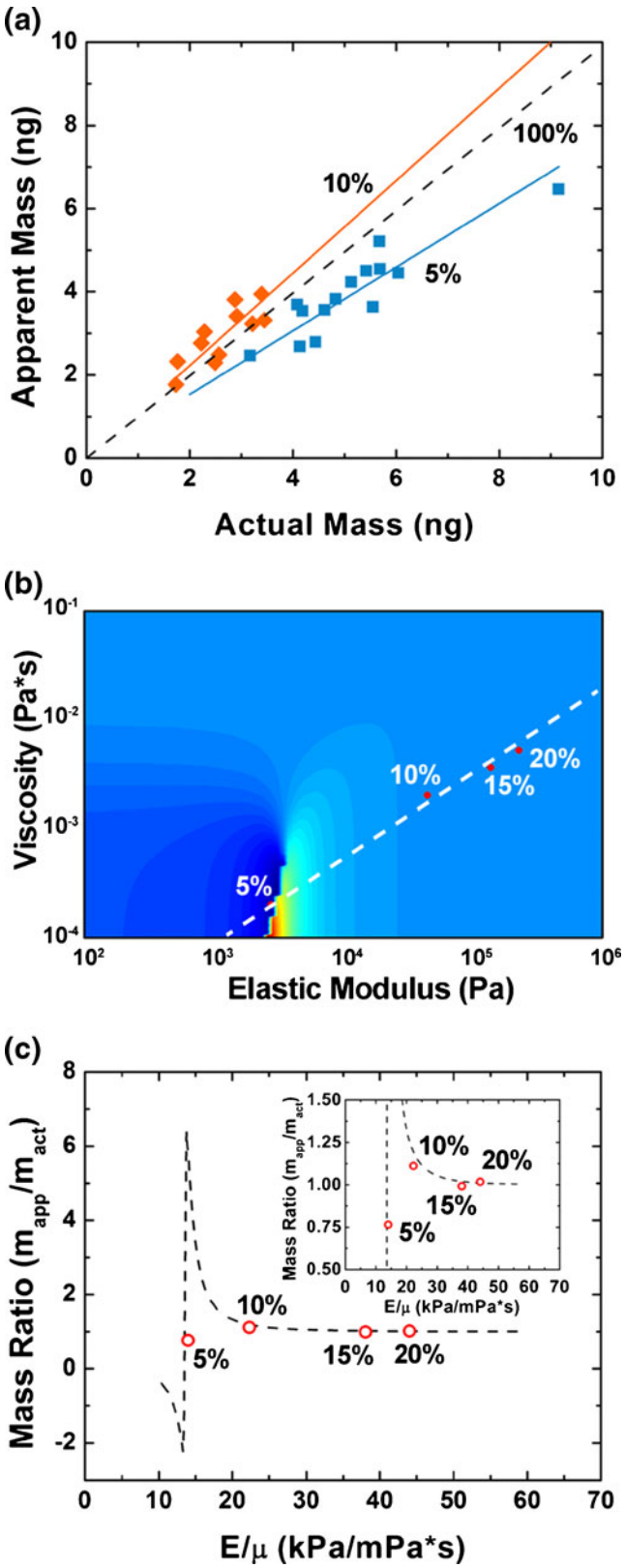

Fig. 4 Results and comparison of the 2DOF model of a Kelvin-Voigt material adhered to the surface of a resonant sensor with the experimental data for the material viscoelasticity on the forced response of the system. **a** Comparison of the apparent mass as estimated from resonant frequency with the actual mass measured from confocal. **b** Top view of 3D model plot shows the locations of the experimental data (red dots) and the white line depicts the 2D slice chosen for figure (c), for the 5% hydrogel a viscosity value of 1.0 mPa-s is assumed. **c** Slice through the model plot showing the mass ratio from the model as a dotted line and the red dots as the experimental data, inset shows zoomed in plot showing good agreement of the data to the model. Note, a viscosity value of 1.0 mPa-s is assumed for the 5% hydrogel

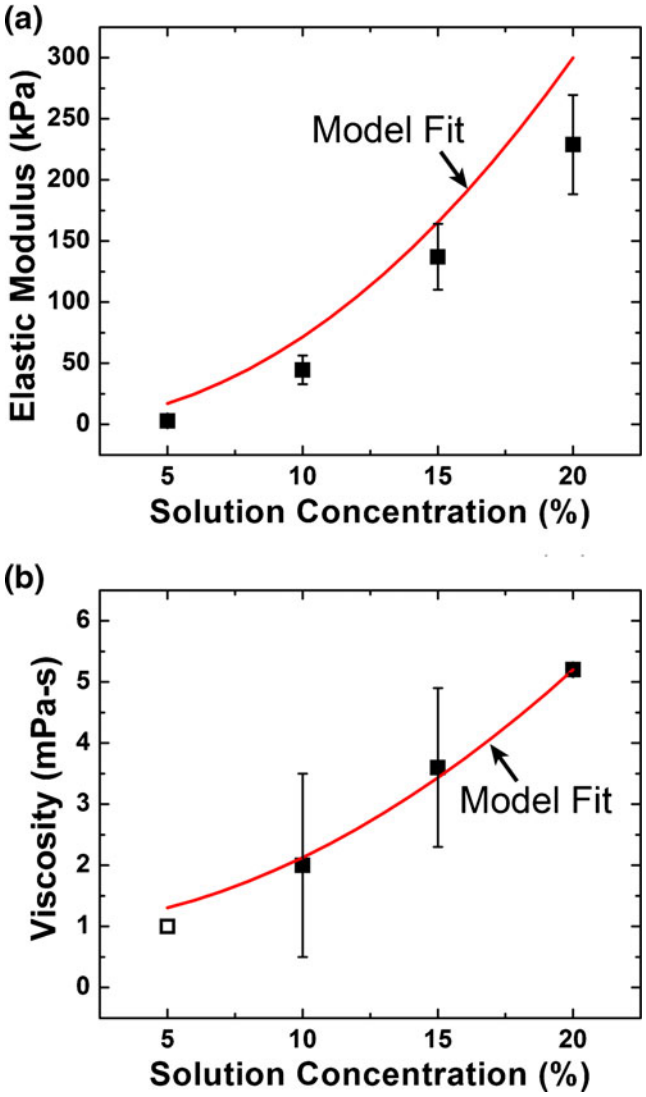

Fig. 5 The viscoelastic properties of hydrogels generally exhibit a power-law dependence on polymer concentration. **a** The predicted power-law fit is plotted alongside the experimental data for the elastic modulus. **b** The predicted power-law fit is plotted alongside the experimental data for the viscosity, the open square indicates the assumed a viscosity value of 1.0 mPa-s for the 5% hydrogel corresponding to water at 20 °C

3 Conclusion

In this work, we have demonstrated the feasibility of using MEMS resonant sensors in estimating the viscoelastic properties of hydrogel microstructures. The technique described here exploits the dependence of the resonance condition of resonant sensors on the mechanical properties of the adhered material. We modeled this dependence through the use of a Kelvin-Voigt 2DOF model, which was shown to accurately predict the experimental behavior. By examining hydrogel microstructures with micromechanical properties varied through polymer concentration, we were able to calculate the power-law behavior of both elasticity and viscosity. These calculated values exhibited excellent agreement with independent measurements using AFM techniques. Ultimately, we have presented a new technique for quantifying the viscoelasticity of nanogram-scale hydrogel structures. This technique was performed in an aqueous environment and may overcome limitations of other techniques, such as dependence on AFM probe characteristics and QCM electrode size. The microscopic lab-on-chip format allows us to explore hydrogel samples on the scale of individual cells, and this technique may be expanded in the future to study the mechanical properties of other biological materials.

4 Experimental section

4.1 Hydrogel preparation

PEGDA (MW 575 g mol^{-1}) and 2,2-dimethoxy-2-phenylacetophenone (DMPA), a photoinitiator, were combined in the ratio of 10 mg DMPA per mL PEGDA to form a stock solution, and the photoinitator was allowed to dissolve for 4 h before use. Lower concentrations were obtained by diluting stock solutions in DI water. Concentrations indicate a volume/volume ratio of stock solution to diluted total. All solution preparation and storage took place in the absence of UV light.

Prior to initiating microstructure deposition, the surface was methacrylated following a previously established protocol. (Dorvel et al. 2010) Chips were cleaned under oxygen plasma for 2 min, then treated in small groups in a 500 mL glass jar. 250 μL of 3-acryloxypropyl trimethoxysilane was pipetted around the base of the jar, after which the jar was sealed and placed in an oven at 80°C for at least 4 h. During baking, the silane vaporizes and deposits on the surface, forming pendant methacrylate groups to promote hydrogel adherence. (Dorvel et al. 2010) Samples were then gently rinsed with acetone and methanol, allowed to air dry, and used within 24 h. The pre-polymer solution was then deposited on the sensors using e-jet printing. After deposition the droplets undergo a free radical polymerization reaction stimulated by 9 W cm^{-2} UV curing spot lamp and become insoluble in the developer. (Jo and Blum 1999)

4.2 Mechanical property characterization with AFM

An MFP-3D Asylum Research (Santa Barbara, CA) AFM was used to characterize mechanical properties using thin film hydrogel samples (70 μm thickness). We used a silicon nitride cantilever with a spring constant of 0.06 N m^{-1} and a 2.5 μm silica spherical indenter to extract force-indentation curves. The elastic modulus of the hydrogel was then

extracted from the region of elastic deformation using the Hertz model:

$$F = \frac{4}{3} E_C R^{1/2} d^{3/2} \tag{1}$$

where F is the magnitude of the loading force, E_C is the effective elastic modulus, R is the radius of the indenter probe, and d is the indentation displacement. However, the effective elastic modulus also includes the elastic effects of the spherical indenter, which must be separated from the elasticity of the sample material using the following equation:

$$\frac{1}{E_C} = \frac{1 - \nu_{gel}^2}{E_{gel}} + \frac{1 - \nu_{glass}^2}{E_{glass}} \tag{2}$$

where E_{gel} and E_{glass} are the elastic moduli of the hydrogel and the glass spherical particle, and ν_{gel} and ν_{glass} are the Poisson ratios of the two materials. The material properties of the spherical particle are 68 GPa and 0.19, as characterized previously by Asylum Research, and we assumed a ν_{gel} of 0.45, as suggested by previous work for hydrogel incompressibility. (Chippada 2009)

Creep indentation measurements with AFM used the same cantilever and indenter tip. A step load was applied to the cantilever probe and the resulting force applied from the cantilever to the sample was held constant through a feedback loop on the cantilever deflection. While the force was held constant, the linear variable differential transformer (LVDT) signal of the AFM was monitored for 10 s to collect a creep curve. Based on the Kelvin-Voigt model, we can derive the following response equation:

$$I(t) = \frac{F_0}{k}\left[1 - e^{-t\frac{k}{\eta}}\right] \tag{3}$$

where $I(t)$ is the indentation as a function of time t, defined as the difference between of the Z-sensor (LVDT) and cantilever deflection, which is held constant. F_0 is the magnitude of the loading force, k is the spring constant of the material, and η is the viscosity of the material. Exponential fitting of the indentation curve returned the material viscosity. All AFM experiments were performed at a room temperature of 22°C.

4.3 Confocal microscopy

We used confocal microscopy to determine volumes and calculate the volumetric mass of the hydrogel microstructures. PEGDA hydrogel microstructures were labeled with fluorescein isothiocyanate-conjugated poly-L-lysine in DI water (50–100 μg mL^{-1}, > 12 h). Prior to imaging, the MEMS sensors with hydrogels were rinsed and immersed in DI water. Confocal image stacks (Z-stacks) were acquired with a Zeiss 710 laser scanning confocal microscope using an Argon laser (488 nm) and a Plan-Apochromat 20x/0.8 objective (Carl Zeiss Microscopy GmbH; Jena, Germany). To ensure that the Z-stacks represented the gel dimensions accurately in three-dimensions, XYZ voxel size (X=0.244 μm, Y=0.244 μm, Z=1.0 μm) was set based on Nyquist criteria (two pixels per actual unit resolution in XYZ).

4.4 Apparent mass measurements with resonant sensor

For each sensor, three different resonant frequencies were measured. The resonant frequency in air was measured to extract the spring constant of each individual sensor and to compensate for minute sensor to sensor differences that may exist from chip fabrication. The resonant frequency (reference frequency for mass measurements) of each sensor in DI water was measured. Then, the gels were deposited on the sensor array and the resonant frequencies and optical images of each selected sensor were collected. With the spring constant and the reference frequency, the measured frequencies were converted to the mass of individual sensors, with and without attached hydrogels, ultimately allowing for the mass of individual hydrogel microstructures to be extracted, using the following equation:

$$m_{gel} = \frac{k}{4_{\pi^2}}\left(f_{wet\_gel}^{-2} - f_{wet\_empty}^{-2}\right) \tag{4}$$

where f_{wet_gel} is the resonance frequency of the sensor with the gel in liquid, f_{wet_empty} is the resonance frequency of the empty sensor, k is the spring constant of the sensor, and m_{gel} is the mass of the gel.

4.5 Estimation of mechanical properties using resonant sensors

The 2DOF model of the resonant sensor system with attached Kelvin-Voigt solid can be described by the following equations of motion:

$$\begin{bmatrix} m_1 & 0 \\ 0 & m_2 \end{bmatrix}\begin{Bmatrix} \ddot{x}_1 \\ \ddot{x}_2 \end{Bmatrix} + \begin{bmatrix} c_1 + c_2 & -c_2 \\ -c_2 & c_2 \end{bmatrix}\begin{Bmatrix} \dot{x}_1 \\ \dot{x}_2 \end{Bmatrix} + \begin{bmatrix} k_1 + k_2 & -k_2 \\ -k_2 & k_2 \end{bmatrix}\begin{Bmatrix} x_1 \\ x_2 \end{Bmatrix} = \begin{Bmatrix} F_0 \\ 0 \end{Bmatrix} e^{i\omega t} \tag{5}$$

For each sensor, the spring constant k_1 and resonant frequency ω_1 are measured (approximately 20 N m^{-1} and 4.0×10^5 radians s^{-1}, respectively), and together are used to calculate the mass of the sensor, $m_1 = k_1/\omega_1^2$ (approximately 125 ng). The coefficient of viscous damping for each sensor, c_1, is estimated to be approximately 9.5×10^{-6} N s m^{-1}.

Given non-dimensional parameters $\Omega=\omega_2/\omega_1$ and $M=m_2/m_1$, Eq. 6 describes the resonance condition of the 2DOF system ($\omega=\omega_2$):

$$D_1 k_2^2 + D_2 k_2 + D_3 + D_4 c_2^2 = 0, \tag{6}$$

where the coefficients are described by:

$$\begin{aligned} D_1 &= \tfrac{1-\Omega^2(1+M)}{k_1^2}, \\ D_2 &= \tfrac{\Omega^2 M\left(2\Omega^2-2+\Omega^2 M\right)}{k_1}, \\ D_3 &= \Omega^4 M^2\left(1-\Omega^2\right), \\ D_4 &= \tfrac{\Omega^2\left(1\Omega^2-\Omega^2 M\right)}{k_1 m_1}. \end{aligned} \tag{7}$$

The structural parameters of the hydrogel in the 2DOF model, k_2 and c_2, are related to the mechanical properties, E and η. For an axially-loaded member of uniform cross-section, this relationship is defined by a shape factor $g=2A/L$, where A is cross-sectional area and L is height. (Gere 1997) However, the hydrogel structures used here are dome-shaped and have varying cross-sectional area, thus we cannot use g alone. To determine an effective shape, the hydrogel was modeled as a series of N thin members arranged in parallel. The number of members used for each sample was determined by the number of slices captured by confocal microscopy, with the height of each equal to the slice thickness, and the cross-sectional area calculated using Amira during volume reconstruction. Each thin member has a shape factor, g_n, which leads to an effective shape factor, g_e:

$$g_e = \left(\sum\nolimits_{n=1}^{N} \frac{1}{g_n}\right)^{-1} \tag{8}$$

In principle, g_e will be different for each hydrogel structure, and can be used to calculate the effective stiffness, k_2, and damping coefficient, c_2:

$$k_2 = g_e \cdot E; \quad c_2 = g_e \cdot \eta. \tag{9}$$

In effect, the mechanical properties of each hydrogel can be estimated using Eq. 6 with appropriate shape factor. However, estimating two unknowns in a nonlinear equation is challenging given a single measurement. Instead, by measuring a number of different hydrogel structures varying in concentration, and assuming the elasticity and viscosity of all samples obey a power-law dependence on concentration, the power-law behavior can be estimated using all samples. For each sample, Eq. 6 can be reformulated as an error term for each sample, y:

$$\begin{aligned} y = (E_0, \eta_0, a,\ b) = D_1 g_e^2 E_0^2 C_h^{2a} + D_2 g_e E_0 C_h^a + D_3 \\ + D_4 g_e^2 \eta_0^2 C_h^{2b} \end{aligned} \tag{10}$$

where E_0 and η_0 are the power-law coefficients for elasticity and viscosity, a and b are the respective power-law exponents, and C_h is the hydrogel concentration. The exponents and coefficients can be found as the parameters that minimize the error term across the entire population of observations, P:

$$\hat{E}_0, \hat{\eta}_0, \hat{a}, \hat{b} = \underset{E_0,\eta_0,a,b}{\operatorname{argmin}} \sum_{p=1}^{P} y_p^2(E_0, \eta_0, a, b) \tag{11}$$

The minimum error was found by iteratively updating each parameter based on the gradient of its error dependence. Solutions were restricted based on the requirement of having vibrations in-phase at resonance.

Acknowledgments The authors are thankful to Dr. Liang Liang (E. I. du Pont de Nemours and Company) for her help on confocal data analysis. E.A.C. was funded at UIUC from NSF Grant 0965918 IGERT: Cellular and Molecular Mechanics and BioNanotechnology.

References

E. A-Hassan, W.F. Heinz, M.D. Antonik, N.P. D'Costa, S. Nageswaran, C.-A. Schoenenberger et al., Biophys J **74**, 3 (1998)
K.S. Anseth, C.N. Bowman, L. Brannon-Peppas, Biomaterials **17**(17), 1647 (1996)
T.P. Burg, M. Godin, S.M. Knudsen, W. Shen, G. Carlson, J.S. Foster et al., Nature **446**(7139), 1066 (2007)
V. Chan, P. Zorlutuna, J.H. Jeong, H. Kong, R. Bashir, Lab on a Chip **10**(16), 2062 (2010)
Chippada U (2009) Non-intrusive Characterization of Properties of Soft Hydrogels, Rutgers, The State University of New Jersey, New Brunswick, NJ
B. Dorvel, B. Reddy, I. Block, P. Mathias, S.E. Clare, B. Cunningham et al., Adv Funct Mater **20**(000274044900010), 87 (2010)
J.L. Drury, D.J. Mooney, Biomaterials **24**(000185037700002), 4337 (2003)
A. Engler, F. Rehfeldt, S. Sen, D. Discher, *Cell Mechanics (Methods in Cell Biology)* (Academic, San Diego, 2007), pp. 521–545
Y.-C. Fung, *Biomechanics: Mechanical Properties of Living Tissues* (Springer, New York, 1981)
J.M. Gere, *Mechanics of Materials*, 4th edn. (PWS Pub Co, Boston, 1997)
A. Gupta, D. Akin, R. Bashir, Journal of Vacuum Science & Technology **B 22**(6), 2785 (2004)
J.H. Jeong, V. Chan, C. Cha, P. Zorlutuna, C. Dyck, K.J. Hsia et al., Adv Mater **24**(000298602300005), 58 (2012)
H. Jo, F.D. Blum, Langmuir **15**(000079541000032), 2444 (1999)
T. Keim, K. Gall, J Biomed Mater Res Part A **92A**(2), 702 (2010)
D. Kim, P. Wong, J. Park, A. Levchenko, Y. Sun, Annu Rev Biomed Eng **11**(1), 203 (2009)
Y.M. Kolambkar, K.M. Dupont, J.D. Boerckel, N. Huebsch, D.J. Mooney, D.W. Hutmacher et al., Biomaterials **32**(1), 65 (2011)
H.J. Kong, E. Wong, D.J. Mooney, Macromolecules **36**(12), 4582 (2003)
N.E. Kurland, Z. Drira, V.K. Yadavalli, Micron **43**(2–3), 116 (2012)
J. Lee, J. Jang, D. Akin, C.A. Savran, R. Bashir, Appl Phys Lett **93**, 1 (2008)
Q.S. Li, G.Y.H. Lee, C.N. Ong, C.T. Lim, Biochem Biophys Res Commun **374**, 4 (2008)
Y. Liang, J. Jeong, R.J. DeVolder, C. Cha, F. Wang, Y.W. Tong et al., Biomaterials **32**, 35 (2011)

Millet LJ, Corbin EA, Free R, Park K, Kong H, King WP et al., Small (2012)
S. Nawaz, P. Sánchez, K. Bodensiek, S. Li, M. Simons, I.A.T. Schaap, PLoS One **7**, 9 (2012)
S. Nemir, H.N. Hayenga, J.L. West, Biotechnol Bioeng **105**, 3 (2010)
G.D. Nicodemus, S.J. Bryant, Tissue Engr Part B-Rev **14**, 2 (2008)
V. Normand, D.L. Lootens, E. Amici, K.P. Plucknett, P. Aymard, Biomacromolecules **1**, 4 (2000)
J.U. Park, M. Hardy, S.J. Kang, K. Barton, K. Adair, D.K. Mukhopadhyay et al., Nat Mater **6**, 10 (2007)
K. Park, J. Jang, D. Irimia, J. Sturgis, J. Lee, J.P. Robinson et al., Lab on a Chip **8**, 7 (2008)
K. Park, L.J. Millet, N. Kim, H. Li, X. Jin, G. Popescu et al., Proceedings of the National Academy of Science **107**, 48 (2010)
K. Park, K. Namjung, D.T. Morisette, N.R. Aluru, R. Bashir, J Microelectromech Syst **21**, 3 (2012)
N.A. Peppas, J.Z. Hilt, A. Khademhosseini, R. Langer, Adv Mater **18**, 11 (2006)
E.A. Phelps, N. Landazuri, P.M. Thule, W.R. Taylor, A.J. Garcia, Proc National Acad Sci **107**, 000275130900011 (2010)
J.H. Pikul, P. Graf, S. Mishra, K. Barton, Y.K. Kim, J.A. Rogers et al., IEEE Sensors J **11**, 10 (2011)
I. Sack, G. Buntkowsky, J. Bernarding, J. Braun, J Am Chem Soc **123**, 44 (2001)
B.V. Slaughter, S.S. Khurshid, O.Z. Fisher, A. Khademhosseini, N.A. Peppas, Adv Mater **21**, 000269936900008 (2009)
T.A. Ulrich, E.M.D. Pardo, S. Kumar, Cancer Res **69**, 10 (2009)
V. Vadillo-Rodriguez, S.R. Schooling, J.R. Dutcher, J Bacteriol **191**, 17 (2009)
J. Yoon, S. Cai, Z. Suo, R.C. Hayward, Soft Matter **6**, 23 (2010)